Journal of Power Sources 213 (2012) 375–381

Contents lists available at SciVerse ScienceDirect

Journal of Power Sources

journal homepage: www.elsevier.com/locate/jpowsour

Analysis of gas products from direct utilization of carbon in a solid oxide fuel cell

Tritti Siengchum [a], Felipe Guzman [b], Steven S.C. Chuang [b,*]

[a] Department of Chemical and Biomolecular Engineering, The University of Akron, 170 University Ave., Akron, OH 44325-3909, USA
[b] Department of Polymer Science, First Energy Advanced Energy Research Center, The University of Akron, 170 University Ave., Akron, OH 44325-3909, USA

ARTICLE INFO

Article history:
Received 13 February 2012
Received in revised form
5 April 2012
Accepted 7 April 2012
Available online 16 April 2012

Keywords:
SOFC
Carbon fuel cell
Thermodynamic calculation
Infrared spectroscopy
CO fuel
Boudouard reaction

ABSTRACT

The evolution of gases from direct utilization of carbon in a solid oxide fuel cell (C-SOFC) was studied by potentiostatic/galvanostatic discharge of a fuel cell with coconut carbon, a carbonaceous material with low ash and sulfur content. Operation of C-SOFC at 750 °C produced less CO and more CO_2 than those predicted by thermodynamic calculation using total Gibbs free energy minimization method. The addition of CO_2 to the anode chamber increased CO formation and maximum power density from 0.09 W cm^{-2} to 0.13 W cm^{-2}, indicating the occurrence of Boudouard reaction ($CO_2 + C \Leftrightarrow 2CO$) coupling with CO electrochemical oxidation on the C-SOFC. Analysis of CO and CO_2 concentration as a function of current and voltage revealed that electricity was mainly produced from the electrochemical oxidation of carbon at low current density and produced from the electrochemical oxidation of CO at high current density. The results suggest the electrochemical oxidation of solid carbon is more mass transfer limited than electrochemical oxidation of CO.

1. Introduction

The direct utilization of solid carbon in a fuel cell (i.e., carbon fuel cell) is an attractive approach for electric power generation. The carbon fuel cell could offer significant advantages including: (i) high energy conversion efficiency, (ii) minimization of NO_x emission due to its operating temperature range of 700–1000 °C, and (iii) the production of a nearly pure CO_2 exhaust stream for the direct CO_2 sequestration. The high-energy conversion efficiency of the carbon fuel cell is a result of the electrochemical oxidation of carbon producing CO_2 ($C + O_2 \rightarrow CO_2$), which could achieve an efficiency ($\eta = \Delta G_T/\Delta H_{298}$) exceeding 100% [1].

The use of carbon as fuel for the fuel cell has been studied with molten salt electrolyte and solid oxide electrolyte fuel cells [2]. The major drawbacks of the molten salt electrolyte fuel cell include equipment corrosion from liquid electrolyte and degradation of the electrolyte due to formation of carbonates during electrochemical oxidation of carbon. In contrast to molten salt electrolyte fuel cell, solid electrolyte fuel cells provide the advantages of using a ceramic solid electrolyte which does not suffer from corrosion or degradation and facilitates integration into stack assemblies. The operating principle of the carbon solid oxide fuel cell (C-SOFC) is the electrochemical oxidation of carbon by oxygen anions (O^{-2}) diffused from cathode through the solid electrolyte to the anode electrode, producing CO_2 (reaction (1)) and CO (reaction (2)). Secondary reactions can also take place on the C-SOFC anode, including the Boudouard reaction [3] (reaction (3)) and electrochemical oxidation of CO producing CO_2 (reaction (4)).

$$C + 2O^{-2} \rightarrow CO_2 + 4e^- \quad (1)$$

$$C + O^{-2} \rightarrow CO + 2e^- \quad (2)$$

$$CO_2 + C \Leftrightarrow 2CO \quad (3)$$

$$CO + O^{-2} \rightarrow CO_2 + 2e^- \quad (4)$$

Recently, researchers have explored the use of secondary reactions to improve the C-SOFC performance by integrating a fluidized bed reactor for the Boudouard reaction of carbon to CO (reaction (3)), and a solid oxide fuel cell for the electrochemical oxidation of the resulted CO [4]. Results from these studies have shown power densities as high as 0.14 W cm^{-2} at 0.5 V and 950 °C can be achieved [5,6]. Despite the attractive power density, the electrochemical oxidation of CO could lead to the reduction of the overall energy conversion efficiency of the C-SOFC as the electrochemical oxidation of carbon producing CO_2 is a four-electron process and that of CO is a two-electron process. Our previous studies reported

* Corresponding author. Tel.: +1 330 972 6993; fax: +1 330 972 5856.
E-mail address: schuang@uakron.edu (S.S.C. Chuang).

0378-7753/$ – see front matter © 2012 Elsevier B.V. All rights reserved.
doi:10.1016/j.jpowsour.2012.04.020

the feasibility of direct power generation from a carbon solid oxide fuel cell (C-SOFC) which could give energy efficiencies as high as 52.9% [7].

This study demonstrates the effect of fuel cell load on the evolution of CO and CO_2 on the C-SOFC operated with coconut carbon, a solid fuel selected because of its low content of ash [8,9] and high electronic conductivity. Results from this study showed the rate of formation of CO and CO_2 increase with decreasing the fuel cell load (i.e., increasing current densities). Analysis of the CO and CO_2 produced at different current densities reveals that at low current density, electricity was produced from the electrochemical oxidation of carbon while CO is consumed to produce electricity at higher current density.

2. Experimental

2.1. Fuel cell fabrication and characterization

Anode-supported fuel cells used in this study consisted of a Ni/YSZ (Yttria-stabilized zirconia) support layer (520 μm, 70 wt% Ni), a Ni/YSZ anode interlayer (21 μm, 50 wt%), a 32 μm YSZ electrolyte, a 21 μm YSZ/LSM cathode interlayer (50 wt% LSM), and a 15 μm LSM cathode layer. The Ni/YSZ anode support, Ni/YSZ anode interlayer, and YSZ electrolyte were fabricated by tape casting slips containing NiO, YSZ (TZ-8Y, Tosoh), binder, dispersants and ethanol. The slips were casted and dried at room temperature for 3 days, laminated, cut into 3.1 cm diameter cells, and sintered at 1000 °C for 4 h and at 1450 °C for 4 h. The YSZ/LSM cathode interlayer (Heraeus CL86-8706A) and LSM layer (Heraeus CL8706) were subsequently screen-printed onto the sintered cells and fired at 1200 °C and 1100 °C, respectively, for 2 h. The anode was further impregnated with an aqueous $AgNO_3$ solution (15 wt% $AgNO_3$) and dried at 85 °C for 2 h. Ag was added to the anode with the purpose of increasing the conversion of CO, as reported in previous studies [10]. The microstructure of the solid oxide fuel cell was characterized by Scanning Electron Microscope (SEM, Quanta 200 FEI) and Energy Dispersive X-Ray Spectroscopy (EDX).

2.2. Fuel cell testing and characterization

The experimental apparatus for fuel cell testing, shown in Fig. 1, consisted of (i) a gas manifold with flow controllers (5850E, Brooks), (ii) the fuel cell placed in a high temperature furnace, (iii) an impedance spectrometer (Solatron 1470E CellTest System), (iv) a gas chromatographer (GC, SRI8610C, SRIGC), and (v) a mass spectrometer (MS, GSD-301 Pfeiffer). The anode side of the fuel cell was attached to one end of a Fe-based steel tube serving both as anode compartment and anode current collector. The fuel cell was sealed to the steel tube with an alumina-based sealant, and loaded with 7 g of coconut carbon in direct contact with the Ni/YSZ anode surface. The cathode side of the cell was coated with an Ag conductive paste (#24469, Alfa-Aesar) and was attached to an Ag strip cathode current collector (99.9% purity, C.C. Silver and Gold Inc.). The area coated with the Ag conductive paste (1 cm^2) was used as the fuel cell active area. The voltage-current density characteristics (V-I curves) of the fuel cell were recorded by the Solatron CellTest System. A 4-port valve in the gas manifold was used to switch the inlet flow between H_2, He, CO or CO_2. The effluent composition of the anode compartment was constantly monitored by GC and MS. The MS response of the gaseous species produced from the fuel cell was converted into concentration profiles by means of a calibration curve, obtained by flowing a calibration gas with known concentrations of H_2, He, CO, and CO_2.

The fuel cell containing the coconut carbon was heated from room temperature to 750 °C at heating rate of 3 °C min^{-1} and

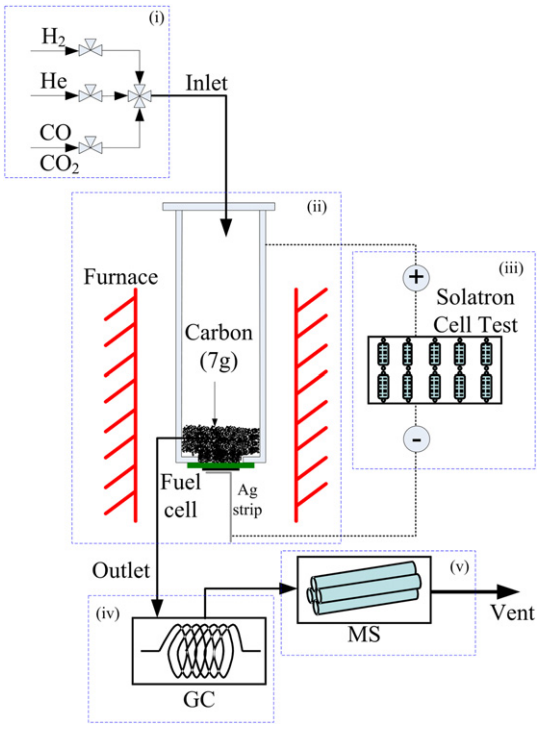

Fig. 1. Experimental apparatus.

reduced at 750 °C for 12 h in flowing H_2/He (265 sccm, 27.2 vol% H_2). The fuel cell was operated at 750 °C with the purpose of ensuring high conductivity of the Fe-based steel anode current collectors. Operating the fuel cell at temperatures higher than 750 °C promotes oxidation of the Fe-based steel, leading to increased Ohmic resistance and low fuel cell performance. The amount of coconut carbon depleted during the fuel cell heating and anode reduction was estimated to be 1 g (0.09 g h^{-1}) from the CO and CO_2 outlet molar flow rates, indicating that sufficient amount of carbon remained in the anode compartment for the carbon fuel cell (C-SOFC) experiments. The effect of the C-SOFC load on the evolution of CO_2 and CO was studied by operating the fuel cell in coconut carbon and pure He (200 sccm), as well as in CO_2/He (210 sccm, 8.6 vol% CO_2) and CO/He (210 sccm, 7.4 vol% CO), recording the V-I curves.

Coconut carbon was produced by pyrolyzing a sample of coconut husks and shell in flowing He at 950 °C. The composition of the coconut carbon was characterized by X-ray Fluorescence (XRF, μEDX 1300, Shimadzu), and Diffuse Reflectance Infrared Fourier Transform spectroscopy (DRIFT). Coconut carbon samples were pyrolyzed in a DRIFT cell to determine surface functional groups on the coconut carbon that produced CO and CO_2. Mixtures of coconut carbon and KBr (120 mg, 5 wt% coconut carbon) were loaded in the DRIFT cell and preheated to 150 °C for 10 min to reduce moisture. The samples were then heated from 50 to 680 °C at a heating rate of 15 °C min^{-1}, and maintained at 680 °C for 10 min in flowing He (10 sccm).

2.3. Equilibrium molar flow rate calculation

The equilibrium molar flow rates at the exhaust of the fuel cell were calculated as a function of current density. The equilibrium molar flow rate of the species *i*, (F_i), is the product of the volumetric flow rate and the concentration of species *i*, derived from molar volume of ideal gas and the corresponding mole fraction (y_j). The

mole fraction of the gaseous products was obtained through the total Gibbs free energy minimization method – an approach for determining the equilibrium composition of a simultaneous multi-reaction system [11–13].

$$G_{\text{system}} = \left(\sum n_j \cdot \left[\Delta G^0_{f,j} + RT\ln\left(y_j P\right)\right]\right)_{\text{gas}} + \left(\sum n_j \cdot \Delta G^0_{f,j}\right)_{\text{condensed}}$$

where,

G_{system} = total Gibbs free energy of the system (J)
n_j = amount of species "j" (mol)
$y_j = n_j/\Sigma n_{j,\text{ gas}}$

The components considered in the C-SOFC anode compartment were CO, CO_2, carbon and O_2 transferred from the cathode. The amount of carbon available for the reactions on the anode of the C-SOFC was assumed to be 1 mg s^{-1} (83.3 μmol s^{-1}) representing the excess amount of carbon required by other reactants. The amount of O_2 transferred from the cathode n_{O_2} at the specific current density can be determined from Faraday's law

$$n_{O_2}\left(\text{mol/s cm}^2\right) = i/Z_{O_2}F$$

where i and F represent current density (A cm^{-2}) and Faraday's constant (96,487 C mol^{-1}), respectively. The initial condition for the Gibbs free energy minimization calculation was $n_{O_2} = 0$ where O_2 is not transferred from the cathode under open circuit voltage conditions (OCV).

3. Results and discussion

Fig. 2 shows the current density and MS profiles of effluents of the C-SOFC recorded at 750 °C and a load of 0.4 V in coconut carbon and the H_2/He, pure He, CO_2/He, and CO/He gas feed. Operating the fuel cell in coconut carbon and the H_2/He gas feed produced a stable current density output of 0.47 A cm^{-2}, consistent with the performance reported in previous studies for anode supported Ni/YSZ anodes in H_2 and carbon fuel [7,14]. Changing the gas feed from He/H_2 to pure He allowed operating the fuel cell exclusively in coconut carbon, causing a rapid decrease in current density output to 0.095 A cm^{-2}, and the simultaneous increase in the MS profiles for CO (m/e = 28) and CO_2 (m/e = 44). This increase in the MS profiles indicates that CO and CO_2 are the main products of the C-SOFC.

Fig. 3 shows the fuel cell V-I curves in coconut carbon recorded after the continuous operation at 0.4 V for 39 min shown in Fig. 2, displaying a maximum power density of 0.09 W cm^{-2} and a maximum current density of 0.27 A cm^{-2}. The C-SOFC power density in this study exceeded those previously reported in the 0.005–0.04 W cm^{-2} range [6,7,14–16]. The rapid decline in the voltage of the V-I curve at current densities above 0.20 A cm^{-2} indicates the occurrence of the mass transfer limitation. The feeding CO_2/He and CO/He to the C-SOFC extend the current density to 0.47 and 0.49 A cm^{-2}. Feeding H_2/He feed (265 sccm, 27% H_2) further increases the maximum current density to 0.86 A cm^{-2} which is smaller than those reported for state of the art Ni/YSZ anode supported fuel cells [17]. The low fuel cell current density can attributed to the use of Fe-based steel current collectors with an area specific resistance of 0.6 Ω cm^2, which contributes a higher resistance than those of high cost precious metal current collectors (i.e., Au, Pt and Pd). The use of Pt current collector with an area specific resistance of 0.1–0.2 Ω cm^2 is expected to increase the maximum power density of our fuel cell by approximately 30% [4,18].

Changing the gas feed from He to CO_2/He increased (i) the OCV from 0.79 to 1.06 V, (ii) the maximum power density from 0.09 to 0.13 W cm^{-2}, and the maximum current density from 0.27 to 0.47 A cm^{-2}. The increase in electric power generation was accompanied by an increase in CO formation, shown by the MS profiles of Fig. 2, suggesting the occurrence of the Boudouard reaction (reaction (3)), and the power generating electrochemical oxidation of CO (reaction (4)). Changing the gas feed from CO_2/He to CO/He resulted in a little variation in the performance of the C-SOFC in Fig. 3, and the CO/CO_2 concentration in Fig. 2, indicating that the rate of reaction (3) is significantly higher than that of reaction (4).

The V–I curve observed in coconut carbon and He feed in Fig. 3 was replotted in Fig. 4 along with the CO and CO_2 molar flow rates resulted from calibration of the C-SOFC MS profiles, and the equilibrium CO and CO_2 molar flow rates from the thermodynamic calculation. The CO and CO_2 molar flow rates obtained from the fuel cell MS profiles under OCV conditions, shown in Fig. 4(b), were produced from pyrolysis of coconut carbon. The coconut carbon reacted with –OH functional group on its surface producing CO and

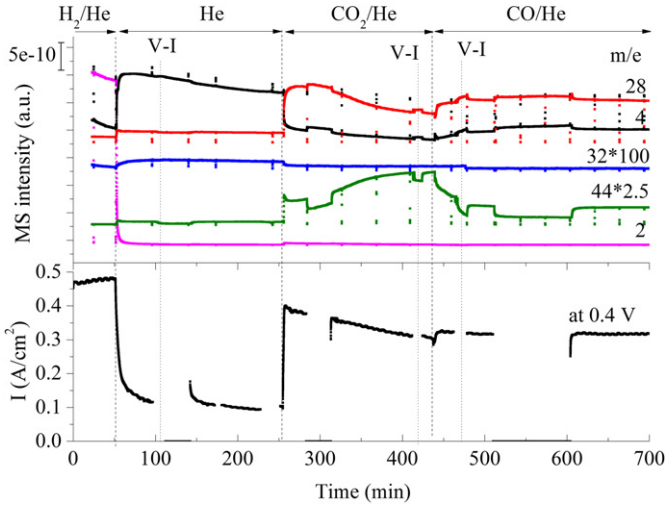

Fig. 2. MS profiles of the C-SOFC effluents and current density recorded at 750 °C and 0.4 V in coconut carbon and a gas feed of H_2/He (265 sccm, 27.2 vol% H_2), pure He (200 sccm), CO_2/He (210 sccm, 8.6 vol% CO_2), and CO/He, (210 sccm, 7.4 vol% CO).

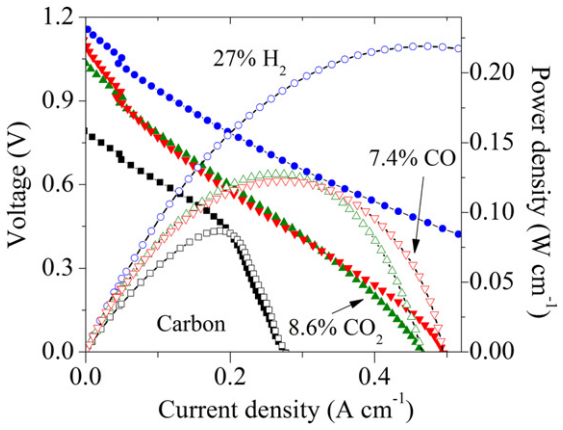

Fig. 3. V-I curves of C-SOFC operated at 750 °C in coconut carbon and a gas feed of He (200 sccm), H_2/He (265 sccm, 27.6 vol% H_2), CO/He (210 sccm, 7.4 vol% CO), and CO_2/He (210 sccm, 8.6 vol% CO_2).

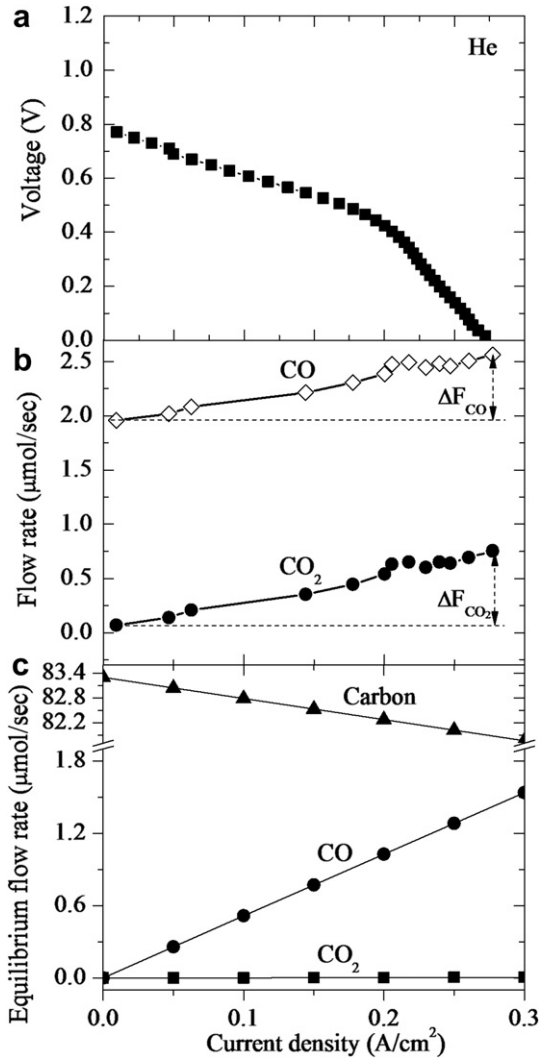

Fig. 4. Plots of (a) voltage, (b) CO and CO_2 effluent molar flow rates, and (c) equilibrium molar flow rates as a function of current density for the C-SOFC operated on coconut carbon and He feed (200 sccm) at 750 °C.

CO_2, as evidenced by IR studies discussed later in a later section. Withdrawing current by applying a load to the C-SOFC initiated the electrochemical oxidation, resulting in increased formation of CO and CO_2. Drawing 0.27 A cm^{-2} increased the CO and CO_2 molar flow rates to 2.56 and 0.75 μmol s^{-1}, respectively, evidencing these species constitute the main byproducts of the C-SOFC.

The equilibrium molar flow rates of carbon, CO and CO_2 as a function of current density, shown in Fig. 4(c), were obtained through minimization of Gibbs free energy considering a stoichiometric C/O^{2-} ratio. The absence of CO and CO_2 molar flow rates at 0 A cm^{-2} reflects the lack of O^{2-} crossing the YSZ electrolyte under OCV conditions. In contrast to the thermodynamic calculation, the experimental data showed that CO and CO_2 were produced at OCV from oxidation of coconut carbon. Hence, it is appropriate to compare the relative increase in the CO and CO_2 flow rates (ΔF_{CO} and ΔF_{CO_2}) obtained when drawing current from the C-SOFC to the equilibrium CO and CO_2 flow rates from the thermodynamic calculation. Fig. 4(b) shows ΔF_{CO} and ΔF_{CO_2} at a current density of 0.27 A cm^{-2} were 0.61 and 0.68 μmol s^{-1} while the predicted equilibrium CO and CO_2 flow rates, shown in Fig. 4(c), were close to 1.40 and 0.01 μmol s^{-1}. The thermodynamic calculation showed CO to be the main product under the fuel cell operating conditions with negligible amounts of CO_2, in agreement with previous research work [11].

The absence of CO_2 at equilibrium can be attributed to the high forward reaction rate of $CO_2 + C \rightarrow 2CO$ at elevated temperatures which can convert majority of CO_2 to CO in the presence of carbon [19]. The high CO_2 molar flow rates observed during the experiment suggest that the C-SOFC did not operate close to equilibrium conditions. Operation of the C-SOFC close to equilibrium conditions (i.e., producing high CO concentrations and negligible CO_2 formation) could be obtained by decreasing the carrier gas flow rate, as reported in our previous work [3]. The increased evolution of CO_2 during the experiment could result from electrochemical oxidation of carbon (reaction (1)) and/or CO (reaction (4)). The contribution of reaction (1) and reaction (4) to the evolution of CO_2 was further investigated by analyzing the C-SOFC performance in CO_2/He and CO/He gas feeds.

Fig. 5 shows the fuel cell V-I curve observed in coconut carbon and the CO_2/He feed as well as the CO and CO_2 molar flow rates resulted from calibration of the C-SOFC MS profiles, and the

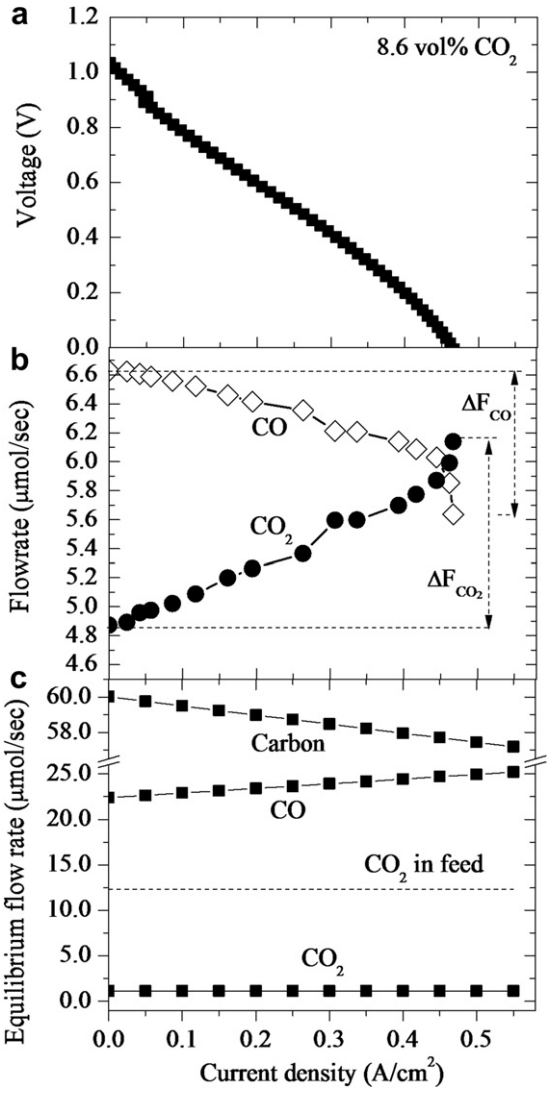

Fig. 5. Plots of (a) voltage, (b) CO and CO_2 effluent molar flow rates, and (c) equilibrium flow rates as a function of current density for the C-SOFC operated on coconut carbon and CO_2/He feed (210 sccm, 8.6 vol% CO_2) at 750 °C.

equilibrium CO and CO_2 molar flow rates from the thermodynamic calculation. Despite the presence of the CO_2/He feed (8.6 vol%. CO_2, 2.4 μmol s^{-1}), CO was the major product from the C-SOFC under OCV conditions with 6.63 μmol s^{-1} of CO and 4.87 μmol s^{-1} of CO_2. This result shows that majority of CO_2 reacted with carbon producing CO at 750 °C, in agreement with the thermodynamic calculation of the equilibrium molar flow rates shown in Fig. 5. Drawing current from the C-SOFC decreased the CO and increased the CO_2 molar flow rate. This observation suggests that the rate of CO_2 formation from electrochemical oxidation of carbon and CO (reaction (1) and (4)) is higher than that of CO formation from Boudouard reaction and electrochemical oxidation of carbon to CO (reaction (2) and (3)).

Fig. 6 shows the fuel cell V-I curves in coconut carbon and the CO/He feed, as well as the CO and CO_2 molar flow rates obtained from calibration of the C-SOFC MS profiles, and the equilibrium CO and CO_2 molar flow rates from the thermodynamic calculation. Exposure of the fuel cell to the CO/He feed (7.4 vol% CO, 10.5 μmol s^{-1}) under OCV conditions produced a molar flow rate of 8.01 and 1.77 μmol s^{-1} for CO and CO_2, respectively. Drawing 0.27 A cm^{-2} resulted in ΔF_{CO_2} of 0.41 μmol s^{-1}, while the outlet CO molar flow rate decreased by 0.06 μmol s^{-1} ($\Delta F_{CO} = -0.06$ μmol s^{-1}). Pursuing mole balance on carbon at 0.27 A cm^{-2} revealed that the amount of consumed CO could only account for 14% of the increase CO_2. This result suggests that at current densities less than 0.27 A cm^{-2}, more than 80% of the electricity was produced from electrochemical oxidation of carbon to CO_2 (reaction (1)). Drawing 0.51 A cm^{-2} caused a rapid decrease in CO ($\Delta F_{CO} = -1.79$ μmol s^{-1}) and an increase in CO_2 ($\Delta F_{CO_2} = 1.74$ μmol s^{-1}) molar flow rates, indicating that at high current densities the C-SOFC produces electricity by electrochemical oxidation of CO. These results are consistent with those of the C-SOFC with CO_2/He feed, showing that the rates of reaction (1) and (4) were higher than those of reaction (2) and (3). Considering that the rate of Boudouard reaction (reaction (3)) was not affected by the applied current, the formation of CO_2 was promoted with increasing current density, a phenomena previously reported during the electrochemical oxidation of CH_4 on Ag catalyst [20,21]. The equilibrium diagram of carbon, CO, and CO_2 as a function of current density in the CO/He feed is shown in Fig. 6(c). Similarly to the equilibrium diagram of C-SOFC in He feed, CO is suggested to be the major product with negligible amounts of CO_2 produced. In contrast to this equilibrium diagrams, the experiment showed evolution of CO_2 and consumption of CO at high current densities, showing that the C-SOFC with CO/He feed was not operated near equilibrium conditions.

Fig. 7(a) shows the CO and CO_2 equilibrium molar flow rates as a function of temperature for the C-SOFC with He feed at a current density of 0.50 and 1.0 A cm^{-2}. The equilibrium calculation indicates that elevating the C-SOFC operating temperature from 500 to 750 °C increases the CO flow rate. At temperatures above 750 °C, CO becomes the dominant product while CO_2 flow rates reaches close to 0.01 μmol s^{-1}. As a result operation of the C-SOFC at lower

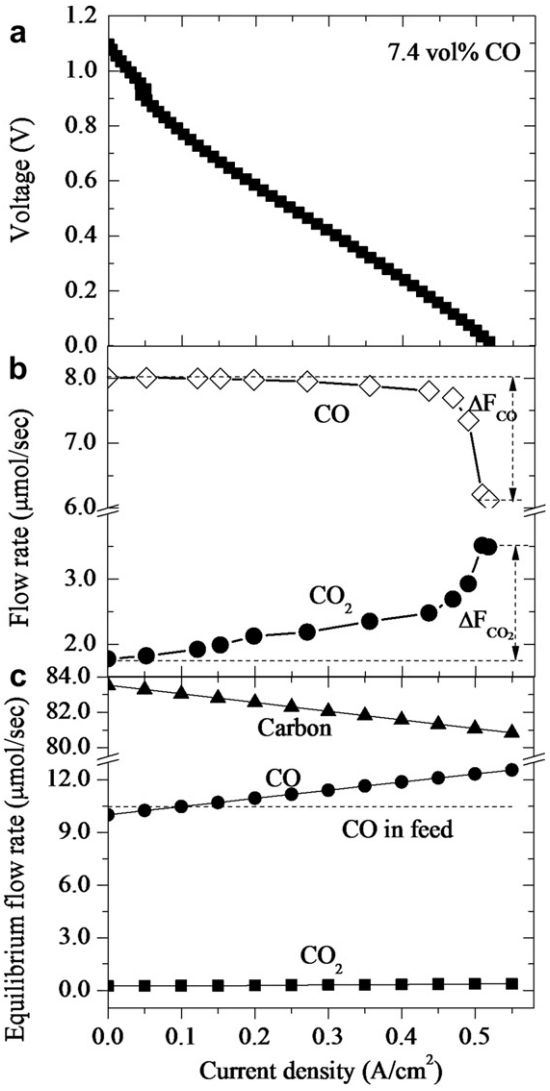

Fig. 6. Plots of (a) voltage, (b) CO and CO_2 effluent molar flow rates, and (c) equilibrium flow rates as a function of current density of the C-SOFC operated on coconut carbon and CO/He feed (210 sccm, 7.4 vol% CO) at 750 °C.

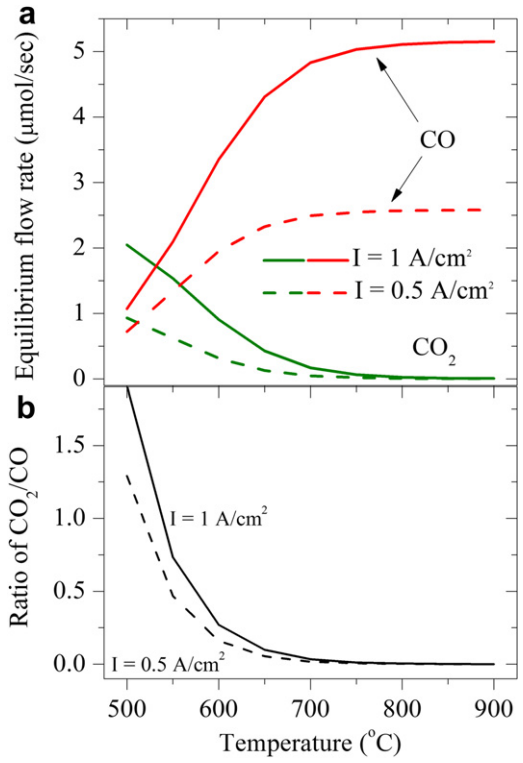

Fig. 7. Plot of (a) CO and CO_2 equilibrium flow rates and (b) ratio of the equilibrium CO_2/CO flow rates as a function of temperature for the C-SOFC operated at 0.5 and 1 A cm^{-2} on carbon with He feed (200 sccm).

temperatures can increase the CO_2/CO molar flow rate ratio. Operation at high current densities (i.e., 1 A cm^{-2}) can also result in higher CO_2/CO ratio as shown in Fig. 7(b), as suggested by previous thermodynamic studies of carbon fuel cells [11]. Evolution of high CO_2/CO molar flow rate ratios benefits the C-SOFC energy conversion efficiency, since electrochemical oxidation of carbon producing CO_2 is a four-electron process and that of CO is a two-electron process [14].

The SEM micrograph in Fig. 8 displays a low porosity surface of the Ni/YSZ anode, which was estimated to be 20.7% by Archimedes method [22]. The relatively low porosity of the fuel cell anode relative to typical porosities of anode supported Ni/YSZ fuel cell (i.e., 35%) was intentionally set during the fabrication procedure with the purpose of enhancing the rigidity of the C-SOFC assembly, as discussed elsewhere [23]. EDX analysis of the Ni/YSZ anode surface shows that Ag particles (0.8–1.2 μm in diameter) were deposited on the Ni particles (2–3 μm in diameter) [24] with a molar ratio of Ag to Ni of 0.1. The composition of the coconut carbon was determined by X-Ray Fluorescence (XRF) prior to the fuel cell experiments, revealing a content of 1.5% of potassium (K) and 0.8% calcium (Ca) considering 3% of ash in coconut carbon. The presence of these alkaline metals in coconut carbon can catalyze formation of CO and CO_2 at elevated temperatures [25], explaining the molar CO and CO_2 flow rates observed during the C-SOFC testing in He feed at OCV conditions (Fig. 4). The evolution of CO and CO_2 from coconut carbon at high temperature was further studied by infrared (IR) spectroscopy. Fig. 9(a) shows the IR absorbance spectra of a sample of coconut carbon recorded at room temperature, displaying the presence of surface C–O, C–H, and O–H functional groups. The presence of these functional groups in coconut carbon is consistent with those reported in previous IR studies of carbon samples [26,27]. Heating the coconut carbon samples in inert He environment to 400, 500, 600 and 680 °C, as the IR absorbance shown in Fig. 9(b), caused the progressive decrease in the intensity of the C–O–H and O–H bands at 1390 and 3160 cm^{-1}, and the simultaneous evolution of CO_2 at 2350 cm^{-1}.

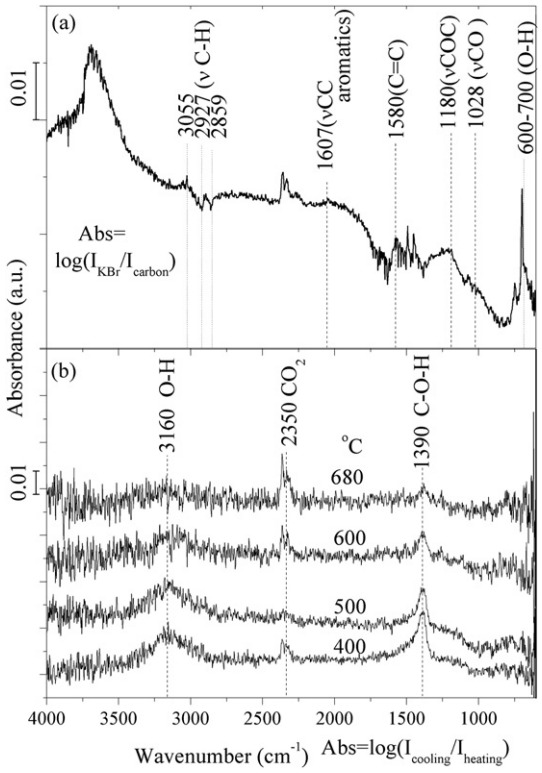

Fig. 9. IR absorbance spectra of coconut carbon (5% in KBr) (a) at room temperature, and (b) during heating to 400, 500, 600 and 680 °C in He environment. Absorbance was obtained by Abs. = log (I_0/I) where I is single beam spectra taken during the heating and I_0 is single beam taken during the cooling at the corresponding temperature.

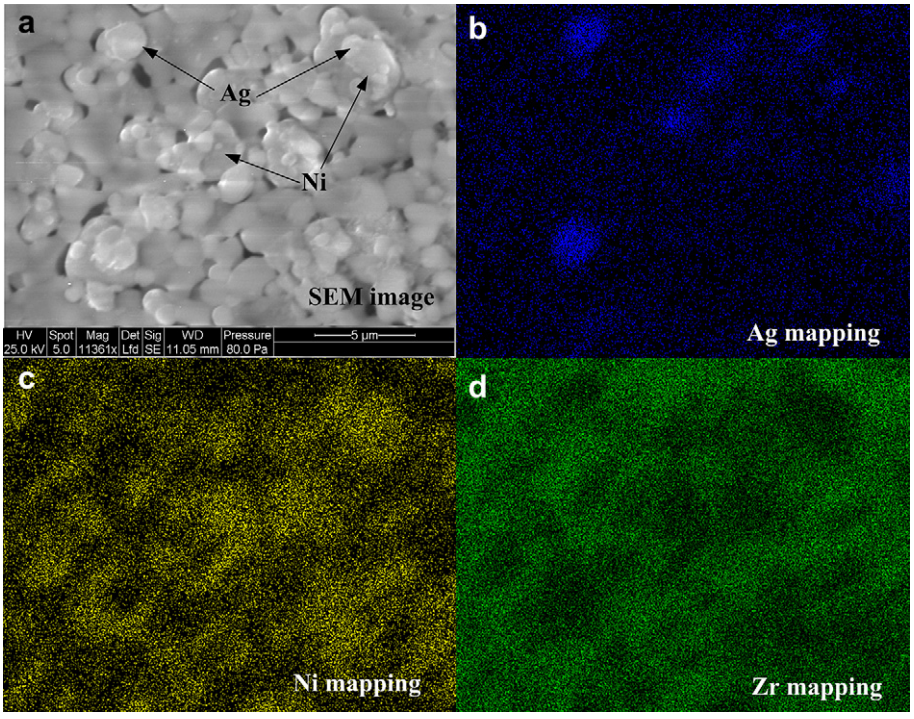

Fig. 8. (a) SEM image of the surface of C-SOFC anode and the corresponding EDX mapping of (b) Ag, (c) Ni, and (d) Zr.

These results suggest that O–H functional group on the surface of coconut coke may react with carbon producing CO and CO_2 which was observed during the operation of C-SOFC at OCV conditions. In addition to the production of CO and CO_2, dissociation of C–O in C–O–H functional group could produce graphite structure and increase the conductivity of the carbon [28]. The electrical conductivity of the coconut carbon was determined to be 0.21 S cm^{-1}, which is comparable to that of highly conductive carbon black [29]. The high conductivity of the coconut carbon could facilitate the transportation of electrons and the electrochemical oxidation of the carbon on the anode.

4. Conclusions

The operation of a solid oxide fuel cell with coconut carbon (C-SOFC) at 750 °C produced a maximum current density of 0.27 A cm^{-2} and produced less CO and more CO_2 from those predicted by thermodynamic calculation. The impact of CO and CO_2 concentration in the anode chamber on the electricity generation was studied by addition of a CO and CO_2 stream. The addition of the CO_2 stream increased CO formation and maximum power density from 0.09 W cm^{-2} to 0.13 W cm^{-2}, indicating the occurrence of Boudouard reaction ($CO_2 + C \Leftrightarrow 2CO$) coupling with CO electrochemical oxidation on the C-SOFC. The contribution of C and CO to the electrical power generation was investigated by analysis of CO and CO_2 concentration at different operating voltage. Reducing the operating voltage shows an increase in CO_2 formation at low current density and rapid consumption of CO at high current density, revealing that at low current density, electricity was produced from an electrochemical oxidation of carbon, while more CO was consumed to produce electricity at higher current density.

Acknowledgments

This work received the financial support from the Department of Energy (DE-FC36-06GO86055), the Ohio Coal Development Office and First Energy Corporation. The authors would like to thank Jak Tanthana and Mehdi Lohrasbi for the fuel cell fabrication.

References

[1] D. Cao, Y. Sun, G. Wang, J. Power Sources 167 (2007) 250.
[2] J.F. Cooper, in: Fuel Cell Sci., Eng. Technol.–2004, 2nd Int. Conf. Fuel Cell Sci., Eng. Technol. (2004), p. 375.
[3] A.C. Chien, S.S.C. Chuang, J. Power Sources 196 (2011) 4719.
[4] C. Li, Y. Shi, N. Cai, J. Power Sources 195 (2010) 4660.
[5] A.C. Lee, S. Li, R.E. Mitchell, T.M. Gur, Electrochem. Solid-State Lett. 11 (2008) B20.
[6] S. Li, A.C. Lee, R.E. Mitchell, T.M. Gur, Solid State Ionics 179 (2008) 1549.
[7] F. Guzman, R. Singh, S.S.C. Chuang, Energy Fuels 25 (2011) 2179.
[8] W.T. Tsai, M.K. Lee, Y.M. Chang, J. Anal. Appl. Pyrol. 76 (2006) 230.
[9] S. Guo, J. Peng, W. Li, K. Yang, L. Zhang, S. Zhang, H. Xia, Appl. Surf. Sci. 255 (2009) 8443.
[10] R.K. Kunkalekar, A.V. Salker, Catal. Commun. 12 (2010) 193.
[11] J.-H. Koh, B.-S. Kang, H.C. Lim, Y.-S. Yoo, Electrochem. Solid-State Lett. 4 (2001) A12.
[12] A. Lima da Silva, I.L. Mueller, J. Power Sources 195 (2010) 5637.
[13] H. Xi, J. Sun, V. Tsourapas, J. Power Sources 165 (2007) 253.
[14] S. Nuernberger, R. Bussar, P. Desclaux, B. Franke, M. Rzepka, U. Stimming, Energy Environ. Sci. 3 (2010) 150.
[15] T.M. Gur, R.A. Huggins, J. Electrochem. Soc. 139 (1992) L95.
[16] R. Liu, C. Zhao, J. Li, F. Zeng, S. Wang, T. Wen, Z. Wen, J. Power Sources 195 (2010) 480.
[17] F. Zhao, A.V. Virkar, J. Power Sources 141 (2005) 79.
[18] S. Lee, G. Kim, J.M. Vohs, R.J. Gorte, J. Electrochem. Soc. 155 (2008) B1179.
[19] M. Homel, T.M. Guer, J.H. Koh, A.V. Virkar, J. Power Sources 195 (2010) 6367.
[20] T. Tagawa, K. Kuroyanagi, S. Goto, S. Assabumrungrat, P. Praserthdam, Chem. Eng. J. 93 (2003) 3.
[21] O.A. Mar'ina, V.A. Sobyanin, V.D. Belyaev, V.N. Parmon, Catal. Today 13 (1992) 567.
[22] I. Gonzalo-Juan, B. Ferrari, M.T. Colomer, A.J. Sánchez-Herencia, J. Membr. Sci. 352 (2010) 55.
[23] A.H.M. Esfakur Rahman, J.-H. Kim, K.-H. Lee, B.-T. Lee, Surf. Coatings Technol. 202 (2008) 2182.
[24] W. Bao, J. Cheng, Z. Hu, S. Jin, Solid State Ionics 181 (2010) 1366.
[25] S.G. Chen, R.T. Yang, J. Catal. 138 (1992) 12.
[26] R. Singh, F. Guzman, R. Khatri, S.S.C. Chuang, Energy Fuels 24 (2010) 1176.
[27] P. Jackson, K. Robinson, G. Puxty, M. Attalla, Energy Procedia 1 (2009) 985.
[28] N.J. Cherepy, R. Krueger, K.J. Fiet, A.F. Jankowski, J.F. Cooper, J. Electrochem. Soc. 152 (2005) A80.
[29] D. Pantea, H. Darmstadt, S. Kaliaguine, L. Sümmchen, C. Roy, Carbon 39 (2001) 1147.